Electronic Supplementary Material (ESI) for Inorganic Chemistry Frontiers.

Supplementary Information

Electrochemical hydrogenation of furfural under alkaline conditions with enhanced furfuryl alcohol selectivity by self grown Cu on Ag electrode

Huiming Wen,[†,a] *Ziyi Fan,*[†,a] *Shuo Dou,*[b] *Jason Chun-Ho Lam,*[c] *Wenjun Zhang,*[a,*] *and Zupeng Chen*[a,*]

[a]Jiangsu Co-Innovation Center of Efficient Processing and Utilization of Forest Resources, International Innovation Center for Forest Chemicals and Materials, College of Chemical Engineering, Nanjing Forestry University, Longpan Road 159, Nanjing 210037, China.

[b]Key Laboratory of Bio-based Material Science and Technology of Ministry of Education, Northeast Forestry University, Harbin, 150040 China

[c]School of Energy and Environment, City University of Hong Kong, Kowloon Tong, Hong Kong SAR 999077, China

[†]These authors contributed equally to this work

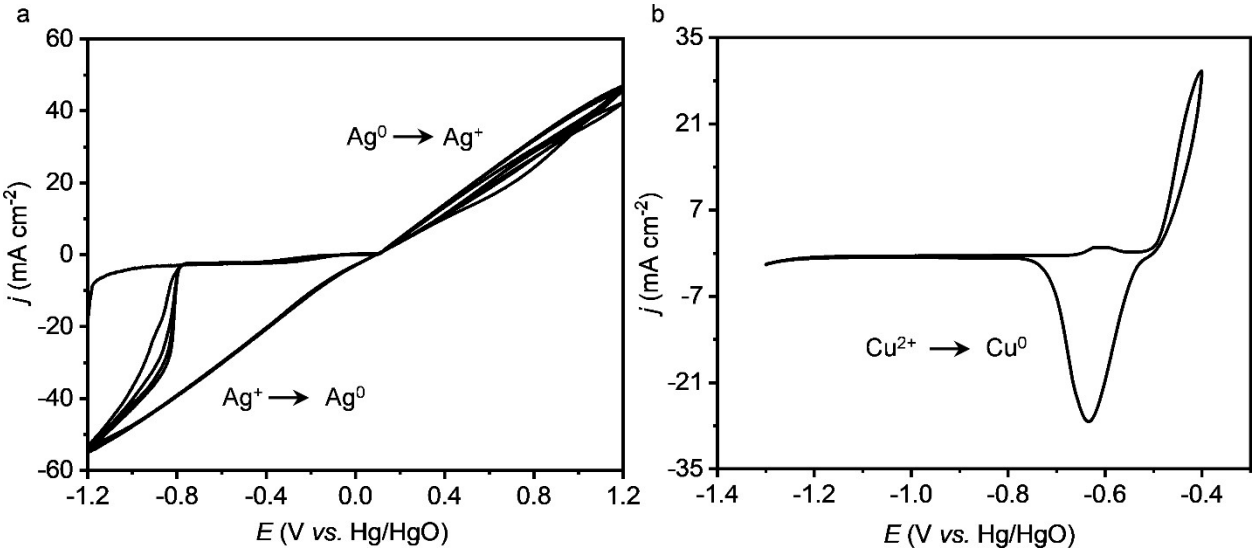

Figure S1. (a) CV curve of Ag foil in 0.1 M NaCl solution. (b) CV curve of P_{Ag} in $Cu(OH)_4^{2-}$ solution.

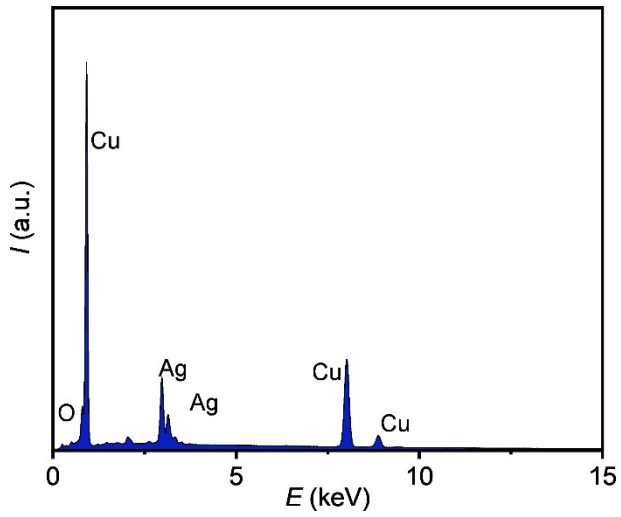

Figure S2. The EDS spectrum of $Cu_{1.15}/P_{Ag}$.

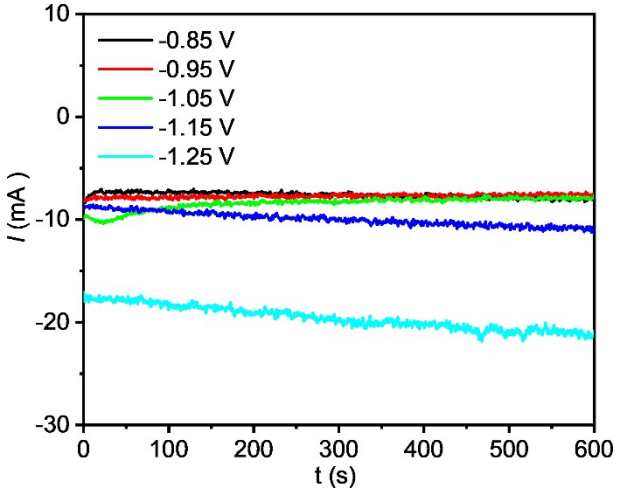

Figure S3 *I-t* curve of electrodeposited Cu.

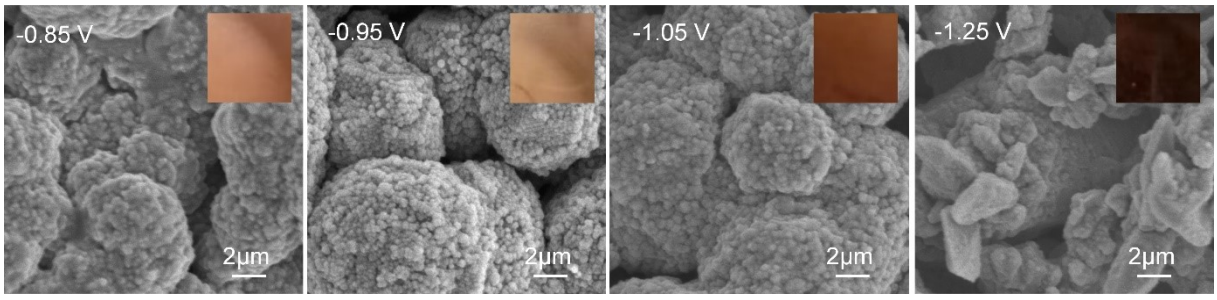

Figure S4. SEM images of P_{Ag} after Cu electrodeposition at different potentials. Insets are the photographs of the corresponding electrodes.

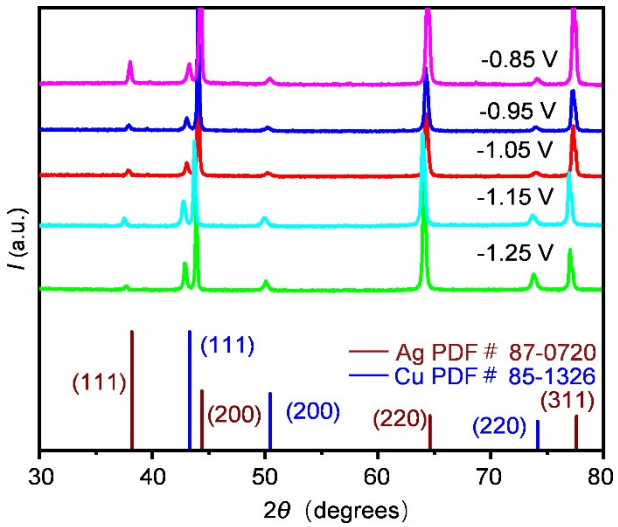

Figure S5. XRD patterns of P_{Ag} after Cu electrodeposition at different potentials.

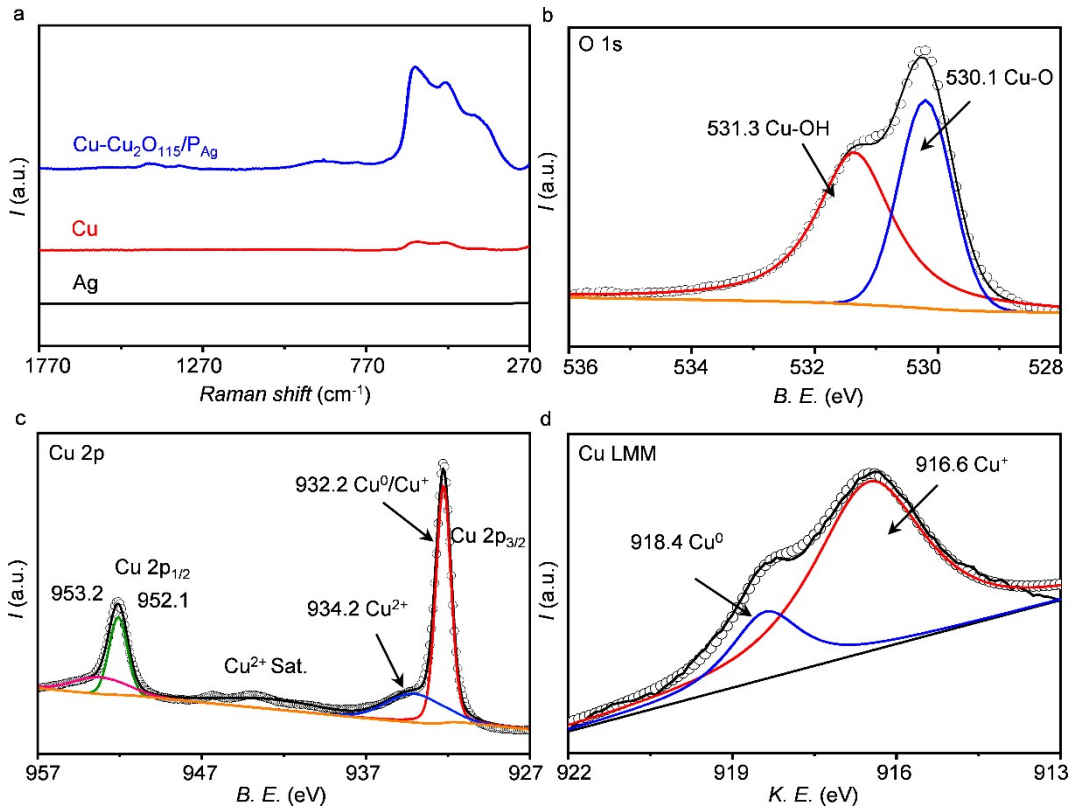

Figure S6. (a) Raman spectra of $Cu_{1.15}/P_{Ag}$, Cu and Ag foil. High-resolution XPS spectra of (b) O 1s, (c) Cu 2p, and (d) Cu LMM spectra of $Cu_{1.15}/P_{Ag}$.

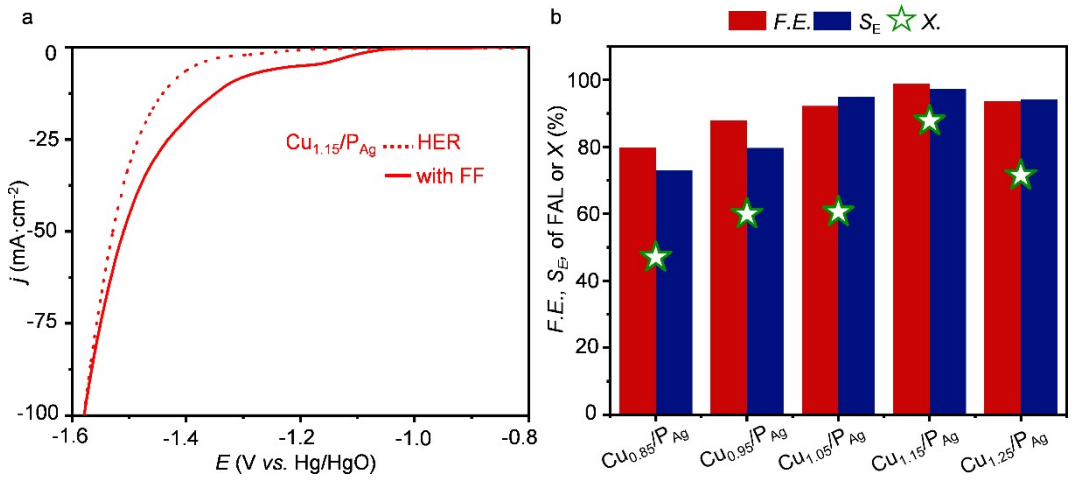

Figure S7. (a) LSV curves of $Cu_{1.15}/P_{Ag}$ in 1 M KOH electrolyte with and without 10 mM FF (HER). (b) The *F.E.*, S_E of FAL, and *X* of FF over P_{Ag} after the electrodeposition of Cu species at different potentials. The electrolytes were 1 M KOH with 10 mM FF, and the electrolytic time was 3 h.

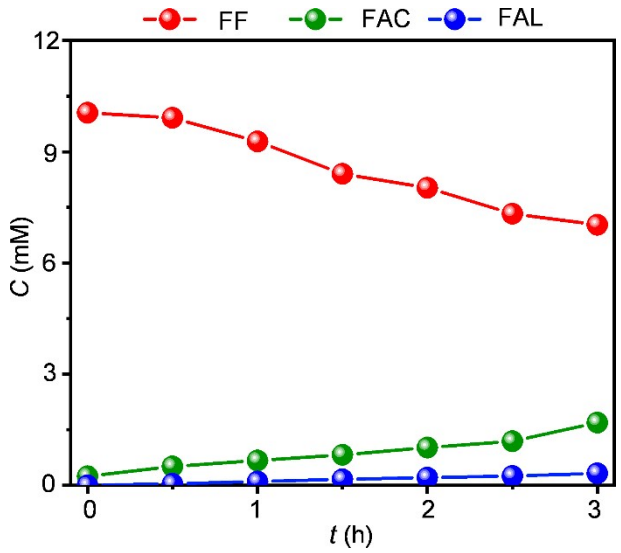

Figure S8. The variation of FF concentration with the increased reaction time under no bias voltage (the initial concentration of FF is 10 mM).

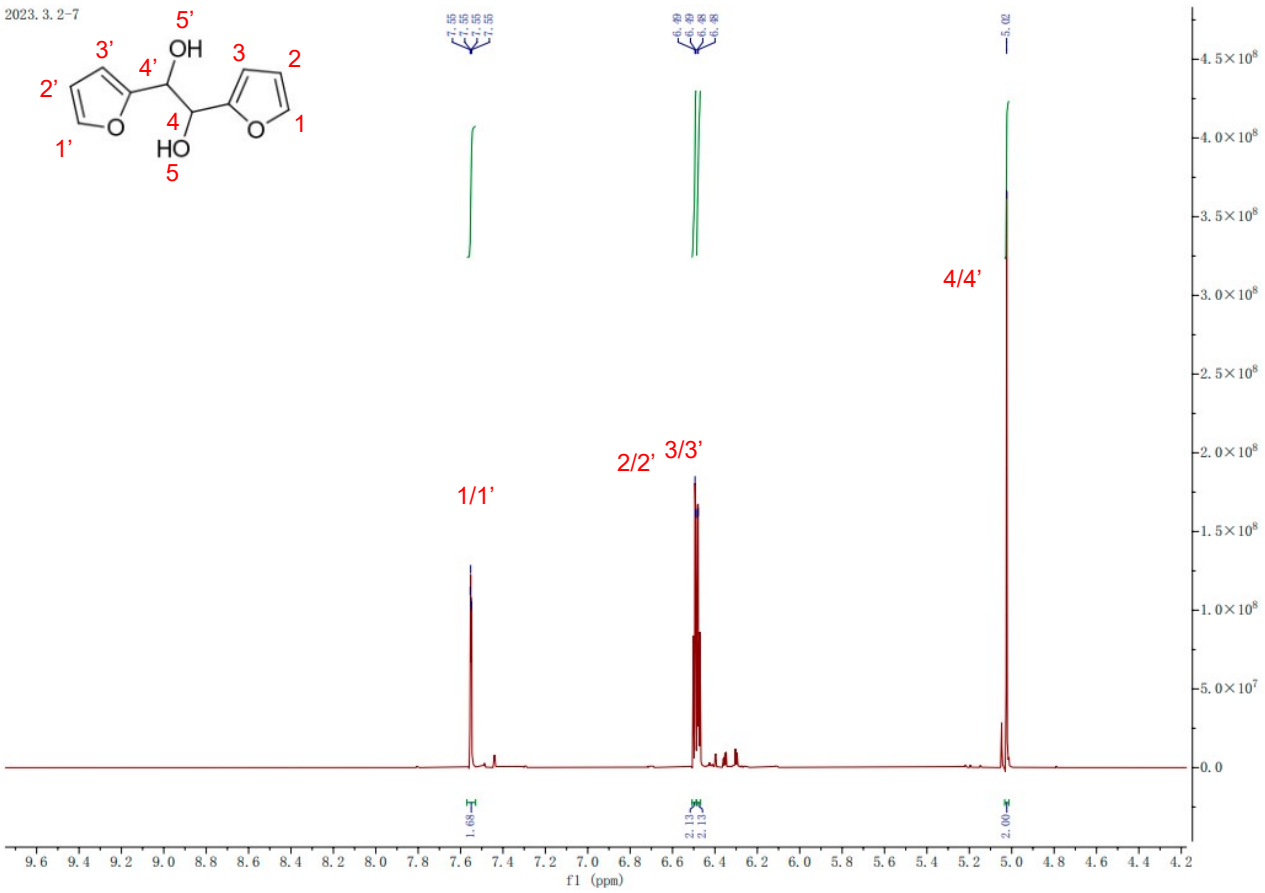

Figure S9. [1]H-NMR image of the home-made HFN.

[1]H-NMR (400 MHz, H_2O+D_2O) δ 7.55 (dd, J = 1.8, 0.8 Hz, 2H), 6.49 (d, J = 0.8 Hz, 2H), 6.48 (d, J = 1.7 Hz, 2), 5.02 (s, 2H).

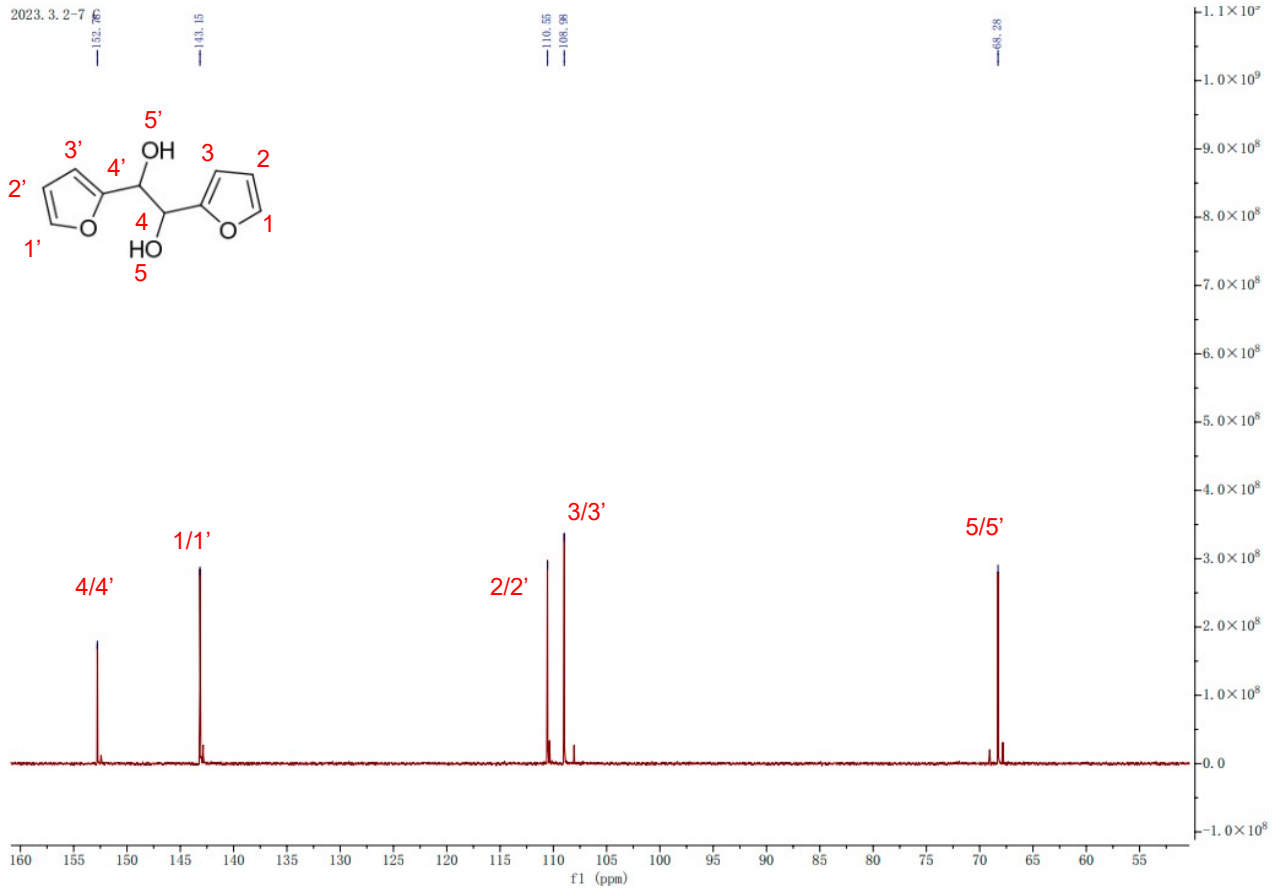

Figure S10. ^{13}C-NMR image of the home-made HFN.

^{13}C-NMR (101 MHz, H_2O+D_2O) δ 152.8 (s), 143.1 (s), 110.6 (s), 109.0 (s), 68.3 (s).

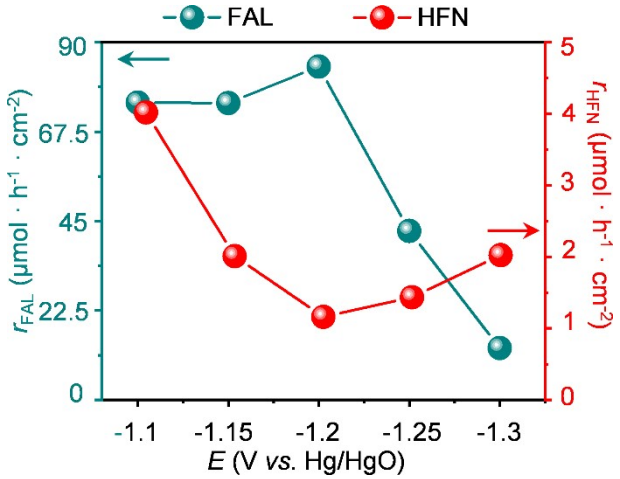

Figure S11. Generation rates of FF and HFN at different voltages over $Cu_{1.15}/P_{Ag}$.

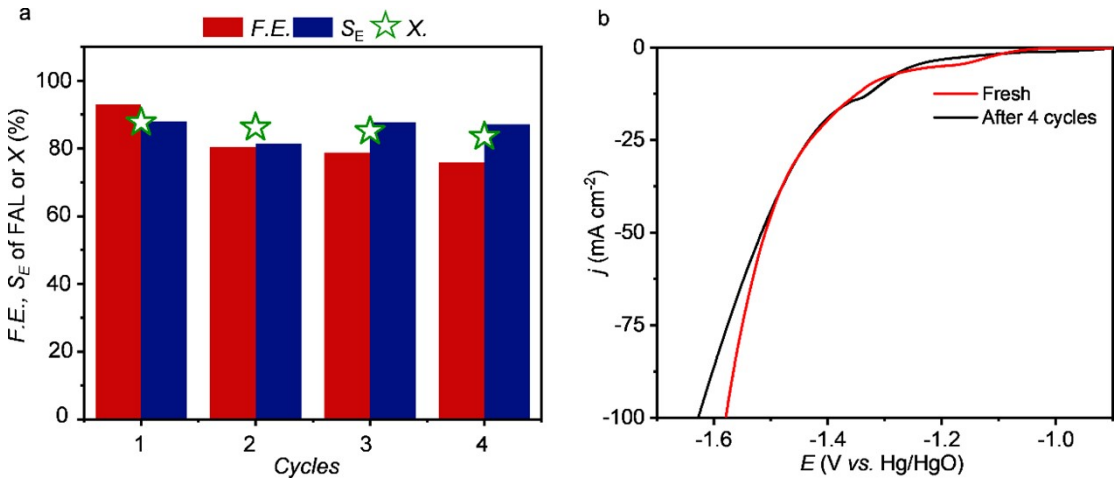

Figure S12. (a) Stability test of $Cu_{1.15}/P_{Ag}$ in 1 M KOH with 10 mM FF at -1.2 V *vs.* Hg/HgO. (b) LSV of fresh and after 4 cycle post catalysts.

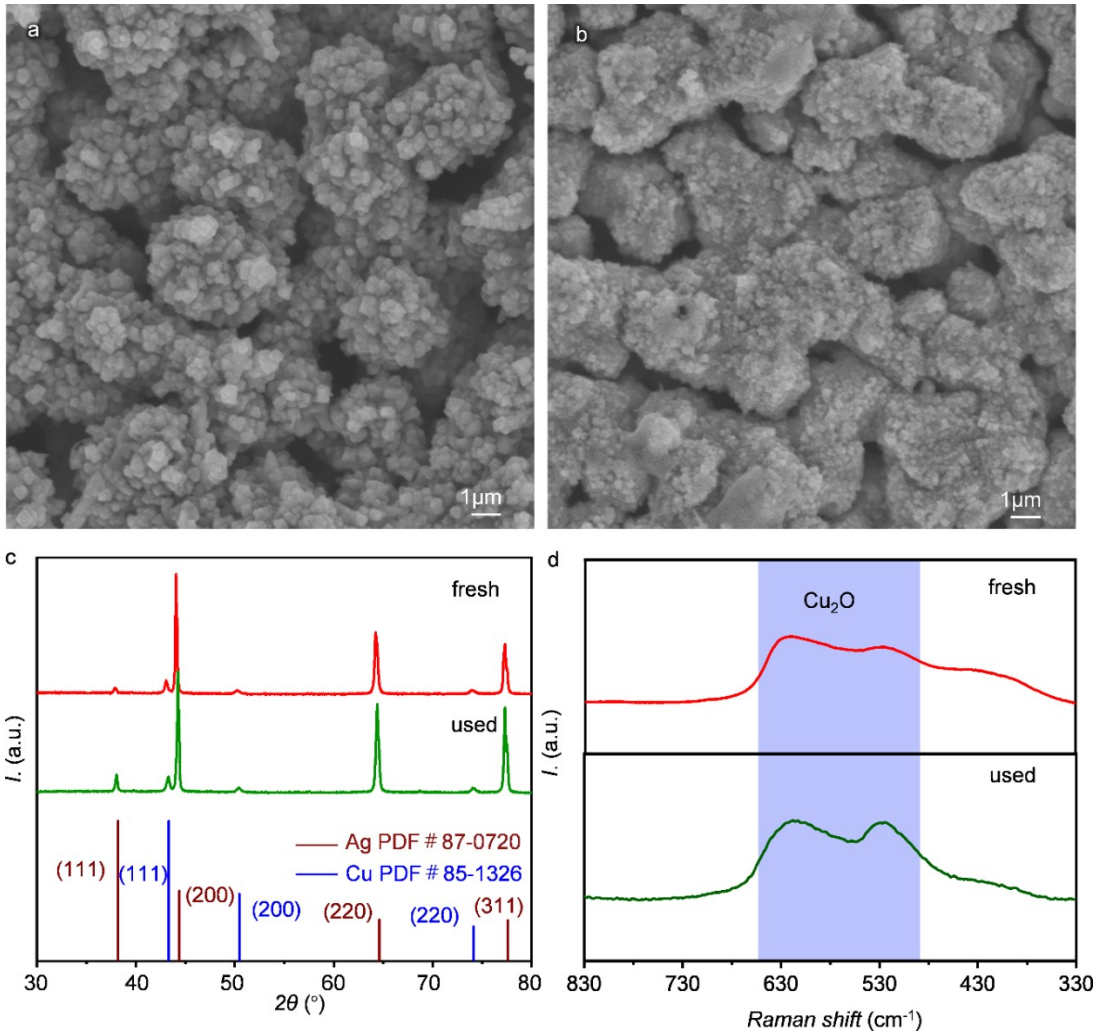

Figure S13. SEM images of $Cu_{1.15}/P_{Ag}$ (a) before and (b) after electrolysis of FF. (c) XRD patterns and (d) Raman spectra of the fresh and used $Cu_{1.15}/P_{Ag}$.

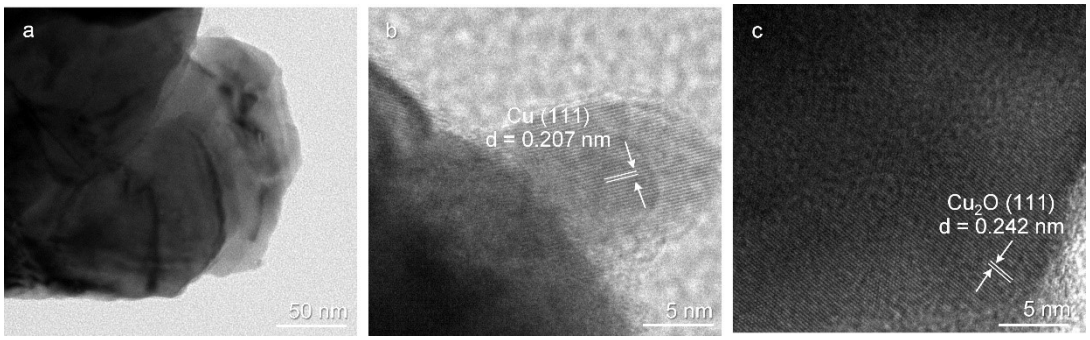

Figure S14. HRTEM images of used $Cu_{1.15}/P_{Ag}$ after electrolysis of FF at different magnifications.

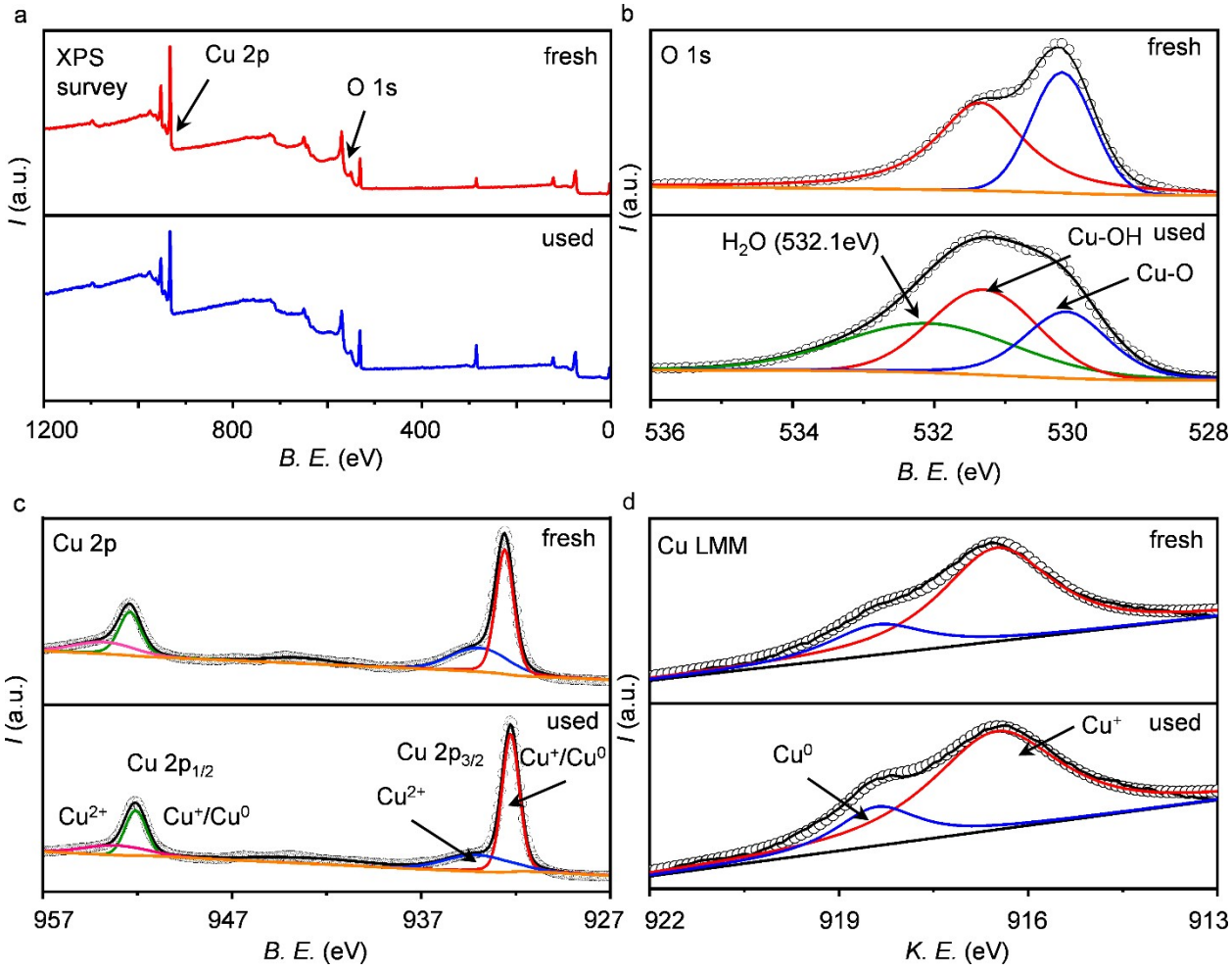

Figure S15. Comparison of the XPS results of the (a) survey, (b) O 1s, (c) Cu 2p, and Cu LMM spectra of the fresh and the used $Cu_{1.15}/P_{Ag}$ after electrolysis of FF.

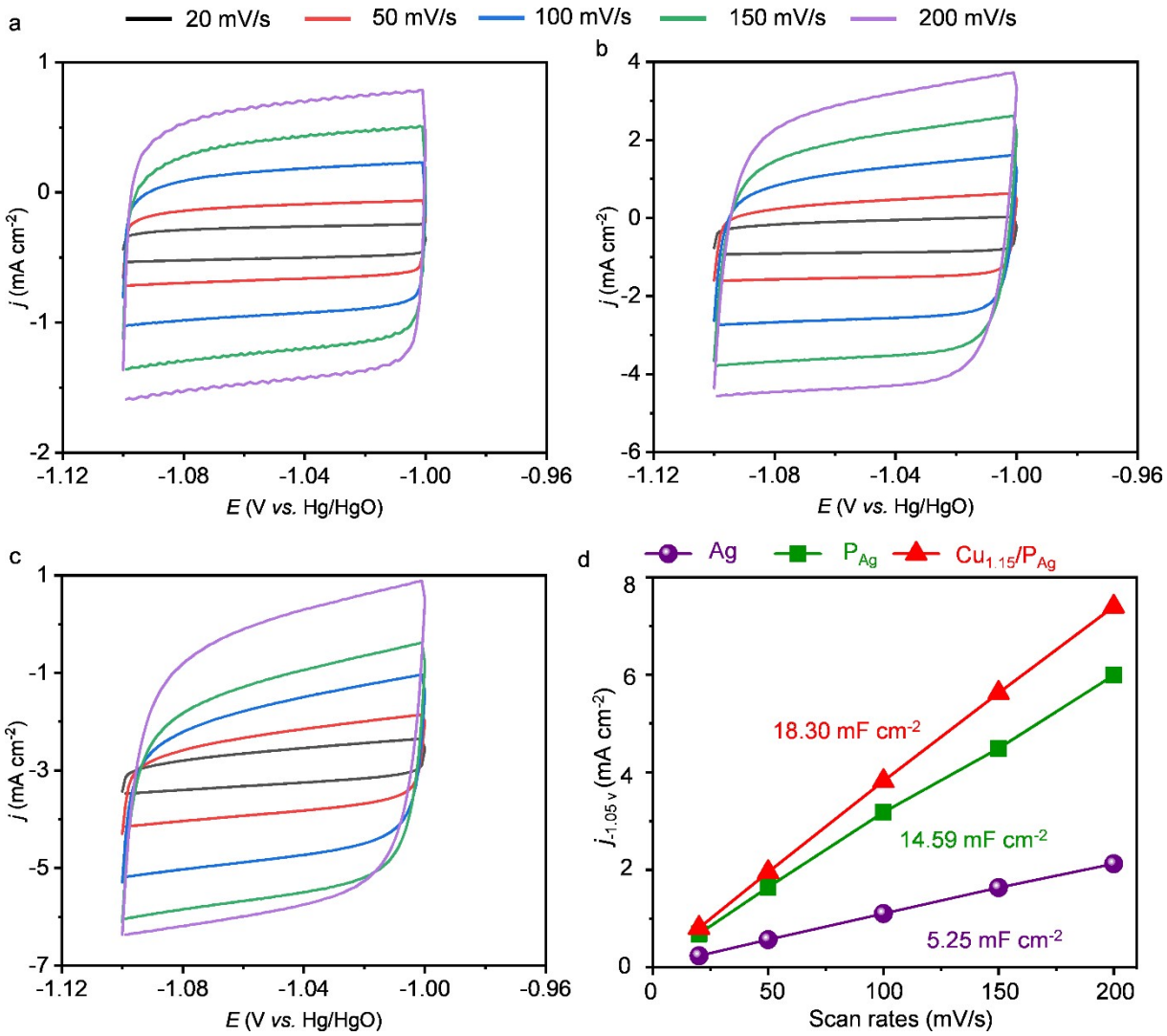

Figure S16. CV curves of (a) bare Ag, (b) P_{Ag}, and (c) $Cu_{1.15}/P_{Ag}$ at scan rates ranging from 20 to 200 mV s^{-1} using 1 M KOH as electrolyte. (d) Relation between current density and scan rates.

The specific capacitance (C_s) was reported as 0.045 mF cm^{-2}.[1] The electrochemically active surface area of Ag, P_{Ag}, and $Cu_{1.15}/P_{Ag}$ were calculated by ECSA = A*C/C_s, where C_s = 0.045 mF cm^{-2}, A = geometric area. The results of the calculations are presented in **Table S2**.

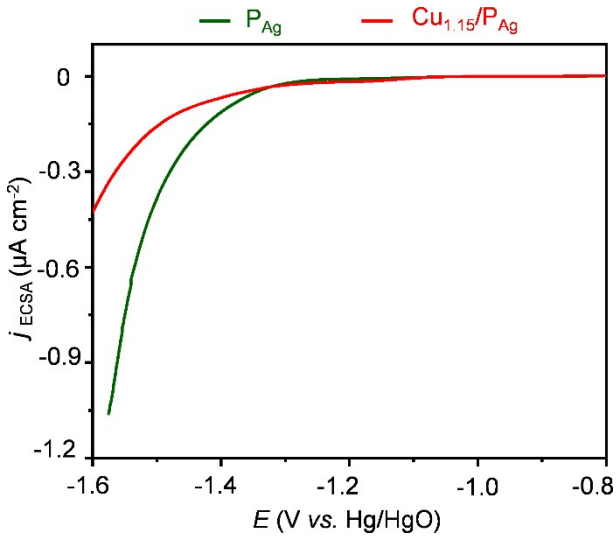

Figure S17. LSV curves of P_{Ag} and $Cu_{1.15}/P_{Ag}$ corrected by ECSA in 1 M KOH electrolyte with 10 mM FF.

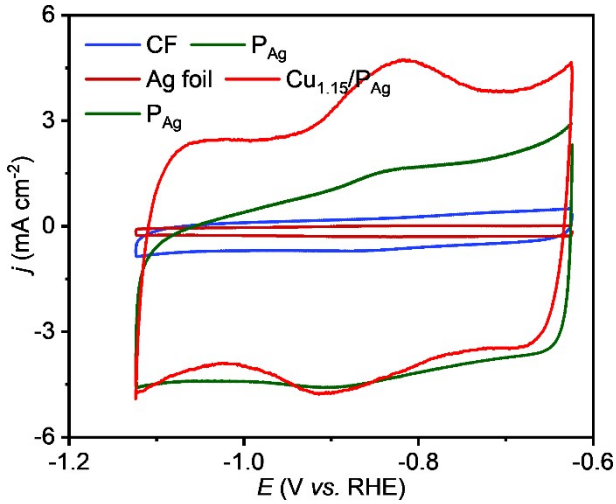

Figure S18. CV curves of CF, Ag foil, P_{Ag} and $Cu_{1.15}/P_{Ag}$ in 1 M KOH electrolyte.

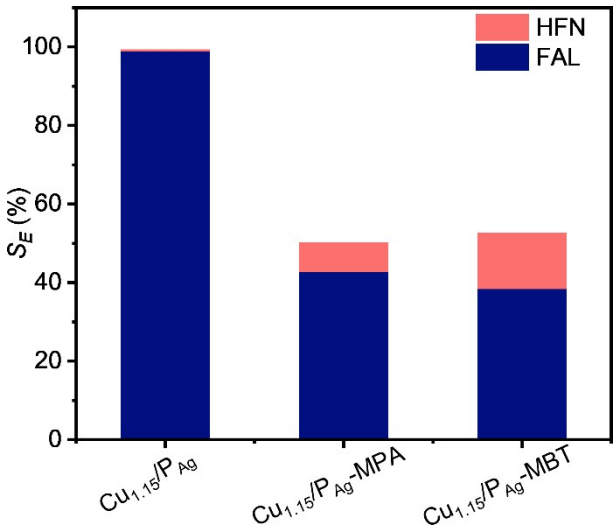

Figure S19. Distribution of HFN and FAL over $Cu_{1.15}/P_{Ag}$ and thiol-treated catalysts (*i.e.*, $Cu_{1.15}/P_{Ag}$-MPA and $Cu_{1.15}/P_{Ag}$-MBT). The electrolyte was 1 M KOH electrolyte containing 10 mM FF, and the electrolysis time was 3 h.

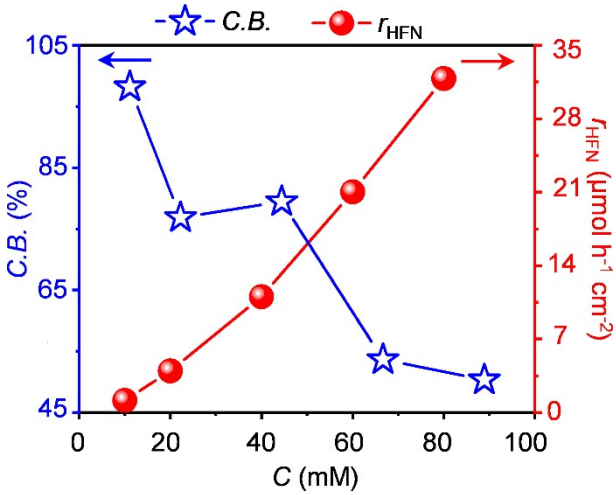

Figure S20. Generation rates of HFN and *C.B.* with different initial FF concentrations over $Cu_{1.15}/P_{Ag}$ in 1 M KOH electrolyte.

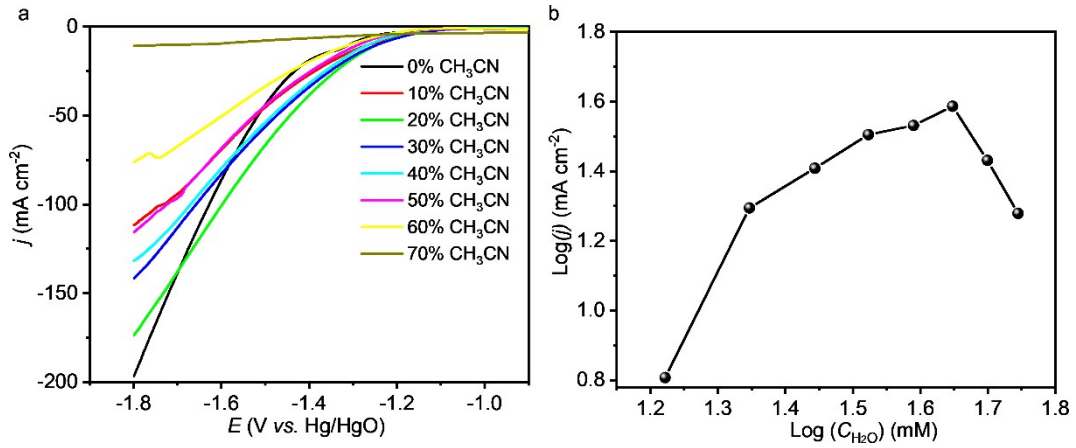

Figure S21 (a) LSV curves of $Cu_{1.15}/P_{Ag}$ in 1M KOH electrolyte containing 10 mM FF with different acetonitrile contents. (b) Correlation curve between water content and current density.

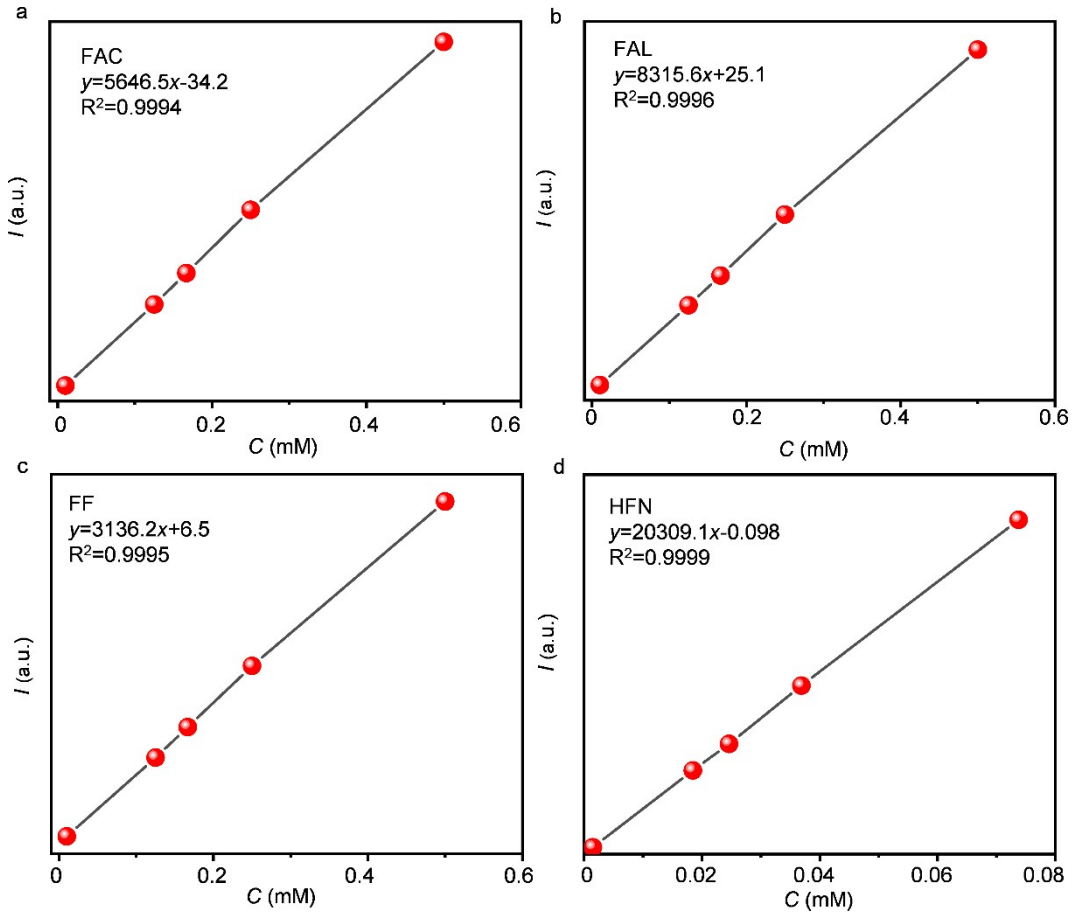

Figure S22. Calibration curves of HPLC for (a) FAC, (b) FAL, (c) FF, and (d) HFN.

Table S1. Quantitative results of $Cu_{1.15}/P_{Ag}$ determined from EDS analysis.

Element	Weight%	Atomic%
O	1.14	4.85
Cu	74.91	80.07
Ag	23.95	15.08

Table S2 Comparison of $Cu_{1.15}/P_{Ag}$ with previously reported Ag- and Cu- based catalysts for the electrocatalytic hydrogenation of FF.

Catalysts	Electrolyte	*E* (*vs.* RHE)	S_{FAL}(%)	$F.E._{FAL}$(%)	Ref
$Cu_{1.15}/P_{Ag}$	**1 M KOH**	**-0.28 V**	**98**	**99**	**This work**
Cu_1/PC	Acetate buffer	-0.75 V	N A	91	2
AgPd/C	Phosphate buffer	-0.5 V	N A	96	3
Cu/C	Acetate buffer	-0.5 V	N A	10	4
$CuPd_{0.021}$/C	0.1 M acetate buffer	-0.58 V	N A	86	5
Cu/graphite	phosphate buffer	N A	86	59	6
Cu_3P/CFC	1 M KOH	-0.35 V	98	98	7
Cu/NC_{900}	1 M KOH	-0.30 V	98	95	8
Cu-NPNi/NF	0.5 M NaOH	-0.45 V	73.2	N/A	9
CuO/Cu	1 M phosphate	-0.25 V	99	91	10
Ag@Cu NWAs/CF	0.5 M borate buffer	-0.88 V	96	96	11

"N A" Representing not available.

Table S3 C_{dl} and ECSA of Ag, P_{Ag}, and $Cu_{1.15}/P_{Ag}$.

Catalysts	C_{dl} (mF cm^{-2})	ECSA (cm^2)
Ag	5.25	116.7
P_{Ag}	14.59	324.2

$Cu_{1.15}/P_{Ag}$	18.30	406.7

Table S4 Fit parameters for the EIS of P_{Ag} in 1 M KOH with different concentrations of FF.

Conc.$_{FF}$	**Rs**	**R_1**	**CPE_1-T**	**CPE_1-P**	**W_1-R**	**W_1-T**	**W_1-P**
10	1.291	29.11	0.005456	0.94286	0.0019645	6.177E-10	0.19731
20	1.289	14.91	0.005416	0.9352	0.0011796	9.126E-9	0.21869
30	1.293	13.03	0.005072	0.93555	0.0012167	9.867E-9	0.21166
40	1.295	8.933	0.004860	0.92359	0.0087302	1.8035E-6	0.20547
50	1.299	7.821	0.004829	0.93465	0.0059218	3.9788E-6	0.21301

Table S5 Fit parameters for the EIS of $Cu_{1.15}/P_{Ag}$ in 1 M KOH with different concentrations of FF.

Conc.$_{FF}$	**Rs**	**R_1**	**CPE_1-T**	**CPE_1-P**	**W_1-R**	**W_1-T**	**W_1-P**
10	1.1	7.795	0.015942	0.956	0.051429	2.195E-9	0.14365
20	1.109	5.709	0.015945	0.94826	0.033263	5.8127E-8	0.16126
30	1.114	5.137	0.015922	0.93295	0.020364	1.0292E-6	0.18851
40	1.119	4.527	0.015359	0.92359	0.015944	6.1727E-6	0.20585
50	1.134	3.849	0.014345	0.92429	0.014856	1.9564E-5	0.21511

Table S6. Experimentally measured and reported Raman shifts in the literature.

	Experimentally measured shift (cm^{-1})	Reported shift (cm^{-1})	Vibrational mode	Vibrational Plane
Cu_2O	625	625[12], 623[13,14]	n.t.[a]	n.t.[a]
	525	525[12], 523[13], 528[14]	n.t.[a]	n.t.[a]
FF	1440	1468[15], 1474[16], 1479[17]	C_1–O_4, C_8–O_4, symmetric bend; C_1=C_2, C_3=C_8 synchronous stretch; C_9–H_{10}, C_1–H_5 asynchronous sway	In-plane
	1342	1374[15],1368[16]	C_9–H_{10}, C_1–H_5 synchronous sway	In-plane
	754	757[16],	C_9=O_{11} sway; C_8–C_9 stretch	In-plane
FAL	801	816[17]	n.t.[a]	n.t.[a]

Reference

1. C. C. L. McCrory, S. Jung, J. C. Peters and T. F. Jaramillo. Benchmarking Heterogeneous Electrocatalysts for the Oxygen Evolution Reaction, *J. Am. Chem. Soc.*, 2013, **135**, 16977-16987.
2. P. Zhou, Y. Chen, P. Luan, X. Zhang, Z. Yuan, S.-X. Guo, Q. Gu, B. Johannessen, M. Mollah, A. L. Chaffee, D. R. Turner and J. Zhang, Selective electrochemical hydrogenation of furfural to 2-methylfuran over a single atom Cu catalyst under mild pH conditions, *Green Chem.*, 2021, **23**, 3028-3038.
3. J. T. Brosnahan, Z. Zhang, Z. Yin and S. Zhang, Electrocatalytic reduction of furfural with high selectivity to furfuryl alcohol using AgPd alloy nanoparticles, *Nanoscale*, 2021, **13**, 2312-2316.
4. U. Sanyal, K. Koh, L. C. Meyer, A. Karkamkar and O. Y. Gutiérrez, Simultaneous electrocatalytic hydrogenation of aldehydes and phenol over carbon-supported metals, *J. Appl. Electrochem.*, 2021,

51, 27-36.

5. P. Zhou, L. Li, V. S. S. Mosali, Y. Chen, P. Luan, Q. Gu, D. R. Turner, L. Huang and J. Zhang, Electrochemical Hydrogenation of Furfural in Aqueous Acetic Acid Media with Enhanced 2-Methylfuran Selectivity Using CuPd Bimetallic Catalysts, *Angew. Chem. Int. Ed.*, 2022, **61**, e202117809.
6. G. Chamoulaud, D. Floner, C. Moinet, C. Lamy and E. M. Belgsir, Biomass conversion II: simultaneous electrosyntheses of furoic acid and furfuryl alcohol on modified graphite felt electrodes, *Electrochimica Acta*, 2001, **46**, 2757-2760.
7. X. Zhang, M. Han, G. Liu, G. Wang, Y. Zhang, H. Zhang and H. Zhao, Simultaneously high-rate furfural hydrogenation and oxidation upgrading on nanostructured transition metal phosphides through electrocatalytic conversion at ambient conditions, *Appl. Catal. B-Environ.*, 2019, **244**, 899-908.
8. W. Xu, C. Yu, J. Chen and Z. Liu, Electrochemical hydrogenation of biomass-based furfural in aqueous media by Cu catalyst supported on N-doped hierarchically porous carbon, *Appl. Catal. B-Environ.*, 2022, **305**, 121062.
9. R. J. Dixit, K. Bhattacharyya, V. K. Ramani and S. Basu, Electrocatalytic hydrogenation of furfural using non-noble-metal electrocatalysts in alkaline medium, *Green Chem.*, 2021, **23**, 4201-4212.
10. Z. Xia, Y. Li, J. Wu, Y.-C. Huang, W. Zhao, Y. Lu, Y. Pan, X. Yue, Y. Wang, C.-L. Dong, S. Wang and Y. Zou, Promoting the electrochemical hydrogenation of furfural by synergistic Cu^{0}–Cu^{+} active sites, *Sci. China Chem.*, 2022, **65**, 2588-2595.
11. Y. Zhong, R. Ren, Y. Peng, J. Wang, X. Ren, Q. Li and Y. Fan, In situ construction of hierarchical Ag-decorated Cu nanowire arrays as an efficient and durable electrocatalyst for hydrogenation of 5-hydroxymethylfurfural and furfural, *Mol. Catal.*, 2022, **528**, 112487.
12 C. G. T. Ho Yeung H. Chan, ‡ and Michael J. Weaver. Oxide Film Formation and Oxygen Adsorption on Copper in Aqueous Media As Probed by Surface-Enhanced Raman Spectroscopy, *J. Phys. Chem. B* 1999**,** ***103***, 357.
13 Y. Deng, A. D. Handoko, Y. Du, S. Xi and B. S. Yeo. In Situ Raman Spectroscopy of Copper and Copper Oxide Surfaces during Electrochemical Oxygen Evolution Reaction: Identification of Cu^{III} Oxides as Catalytically Active Species, *ACS Catal.*, 2016, ***6***, 2473-2481.

14 G. Niaura. Surface-enhanced Raman spectroscopic observation of two kinds of adsorbed OH− ions at copper electrode, *Electrochim. Acta*, 2000, **45**, 3507-3519.

15 J. Thuriot-Roukos, R. Khadraoui, S. Paul and R. Wojcieszak. Raman Spectroscopy Applied to Monitor Furfural Liquid-Phase Oxidation Catalyzed by Supported Gold Nanoparticles, *ACS Omega*, 2020, **5**, 14283-14290.

16 F. Wan, H. Shi, W. Chen, Z. Gu, L. Du, P. Wang, J. Wang and Y. Huang. SERS-Based Flavonoid Detection Using Ethylenediamine-β-Cyclodextrin as a Capturing Ligand, *Nanomaterials,* 2017**, 7** (8), 210

17 K. M. a. K. HAN. Study of the raman effect of organic substances. Part iii. Raman effect of α-mono-derivatives of furan. *Bull. Chem. Soc. Jpn.* 1934, ***9***, 327-344.